Effects of model definitions and parameter values in finite element modeling of human middle ear mechanics

Effects of model definitions and parameter values in finite element modeling of human middle ear mechanics

Daniel De Greef*[1], Felipe Pires[1,2], Joris J. J. Dirckx[1]

[1] Laboratory of Biophysics and Biomedical Physics, University of Antwerp, Groenenborgerlaan 171, 2020 Antwerp, Belgium

[2] Laboratory of Vibration and Acoustics, Federal University of Santa Catarina, Campus Universitário, Trindade, 88040-900 Florianópolis, Brazil

Accepted for publication in Hearing Research on 22 Nov 2016 (DOI: 10.1016/j.heares.2016.11.011)

Abstract

Background: *Despite continuing advances in finite element software, the realistic simulation of middle ear response under acoustic stimulation continues to be challenging. One reason for this is the wide range of possible choices that can be made during the definition of a model. Therefore, an explorative study of the relative influences of some of these choices is potentially very helpful.*

Method: *Three finite element models of the human middle ear were constructed, based on high-resolution micro-computed tomography scans from three different human temporal bones. Interesting variations in modeling definitions and parameter values were selected and their influences on middle ear transmission were evaluated. The models were compared against different experimental validation criteria, both from the literature and from our own measurements. Simulation conditions were restricted to the frequency range 0.1 – 10 kHz.*

Results: *Modeling the three geometries with the same modeling definitions and parameters produces stapes footplate response curves that exhibit similar shapes, but quantitative differences of 4 dB in the lower frequencies and up to 6 dB around the resonance peaks. The model properties with the largest influences on our model outcomes are the tympanic membrane (TM) damping and stiffness and the cochlear load. Model changes with a small to negligible influence include the isotropy or orthotropy of the TM, the geometry of the connection between the TM and the malleus, the microstructure of the incudostapedial joint, and the length of the tensor tympani tendon.*

Conclusion: *The presented results provide insights into the importance of different features in middle ear finite element modeling. The application of three different individual middle ear geometries in a single study reduces the possibility that the conclusions are strongly affected by geometrical abnormalities. Some modeling variations that were hypothesized to be influential turned out to be of minor importance. Furthermore, it could be confirmed that different geometries, simulated using the same parameters and definitions, can produce significantly different responses.*

Abbreviations: ME: middle ear – TF: transfer function – FE: finite element – TB: temporal bone – µCT: micro-computed tomography – TM: tympanic membrane – PT: pars tensa – PF: pars flaccida – TMC: tympanomallear connection – M: malleus – I: incus – S: stapes – IMJ: incudomallear joint – ISJ: incudostapedial joint – SAL: stapedial annular ligament – TT: tensor tympani – SM: stapedius muscle – SFP: stapes footplate

Key words: middle ear - finite element model - tympanic membrane - eardrum – damping – hearing mechanics

[*]**Corresponding author:**

Email address: daniel.degreef@uantwerpen.be

URL: www.uantwerp.be/bimef

Phone number: +32 (0)3 265 34 35

Highlights

- Middle ear transmission was numerically simulated for 3 different geometries
- The 3 geometries with identical parameters produce strongly different outcomes
- Cochlear impedance values differ between sources, but are very influential
- The eardrum loss factor should not be 50% or higher
- Some seemingly important features are actually of marginal influence.

1 Introduction

The development of a finite element (FE) model of the human middle ear (ME) is not straightforward. Many choices need to be made by the researcher, from the early stages of temporal bone imaging and the construction of the geometry, to the choice of physics to be included in the model, the applied material parameters, and the boundary conditions. Since the mechanics of the system are complicated, it is often very difficult to accurately and confidently predict the consequences of the possible choices that need to be made. This results in different model definitions for different research groups throughout the research community (De Greef et al., 2014a; Fay et al., 2006; Ferrazzini, 2003; Gentil et al., 2014; Hoffstetter et al., 2010; Homma et al., 2010; Tuck-Lee et al., 2008; Zhang and Gan, 2011a; Zhao et al., 2009).

In this paper, the aim is to determine the importance of some of the choices made throughout the development of a middle ear FE model. This was done by studying the influence of different variations in the model description on the transfer function (TF) of three different FE models, based on the geometries of three different temporal bones. In addition, by applying the same model definitions to different human ME geometries, this study will bring insight into the isolated effect of geometry on the sound transmission of the ME.

2 Materials and methods

2.1 Study strategy

After evaluating the variations that are described further on, a final model description was constructed that represents a trade-off between agreement with experiments, structural/morphological observations, effort necessary to implement, and computational cost. For example, if a certain feature did not produce a significant change but improves the resemblance to microstructural observations, it was included in the model only if the required effort to implement it and the additional computational

cost were relatively small. An example of this is the incudostapedial joint (ISJ) microstructure (see results and discussion).

Sections 2.2 and 2.3 describe how the final models, referred to as the 'base models' of this paper, were built and defined and which material parameters were used in them. Since three geometries from three different donors were constructed, there are three base models and most variations were studied for all three geometries.

2.2 Geometry

The three temporal bones (TB's) used in this study were a subset of the six TB's used for the morphologic study in De Greef et al. (2015). Therefore, all procedures up to and including the image segmentation are identical to that paper and only a condensed description of the procedures is provided here. Samples 1, 2, and 3 from the current paper are samples 2, 3, and 4 from De Greef et al. (2015), but we will use numbers 1, 2, and 3 from here on in this paper. Some morphological parameters for the three samples are listed in Table 1 to allow the reader to appreciate how the geometries vary. The geometries were selected so that they represent a large (sample 1), small (sample 2), and average (sample 3) ME from our population of six samples.

Table 1: Selection of relevant morphological parameters of the three selected samples. The last column contains statistical parameters from the dataset of 6 samples in De Greef et al. (2015).

Parameter	Sample 1	Sample 2	Sample 3	Mean ± St. Dev. (N=6)
TM surface area (mm^2)	65.9	58.1	60.0	59.4 ± 6.9
IM joint angle (°)	22.5	15.8	12.5	17.5 ± 4.4
IM complex volume (mm^3)	27.6	23.5	23.8	26.7 ± 2.4
Stapes volume (mm^3)	1.44	1.18	1.23	1.24 ± 0.13

The three fresh human TB samples were acquired from Cochlear Technology Centre Belgium. Samples 1 (male, 75y) and 2 (male, 73y) are right TB's; sample 3 (male, 73y) is left. The samples were stained using phosphotungstic acid (PTA) before they were imaged using a micro-computed tomography (μCT) system at the Centre for X-ray Tomography of Ghent University (UGCT) facility (Masschaele et al., 2007). The resulting dataset of the scans had an isotropic voxel pitch of 18.5 μm

(sample 1) or 22.8 μm (samples 2 and 3). After 2D-reconstruction of the μCT scans, the image data were segmented using Amira® 6.1 (FEI Visualization Sciences Group, Hillsboro, Oregon, USA). The segmentation procedure was a combination of automatic and manual segmentation tools and is described in more detail in De Greef et al. (2015). The influence of segmentation operator bias was investigated by Buytaert et al. (2014) and the authors concluded that the results of a manual segmentation are only marginally dependent on the operator.

After image segmentation, the labeled volumes were converted into triangulated surface models using a generalized marching cubes algorithm (Hege et al., 1997). Initially very fine (more than 1M triangles), the surfaces were simplified and remeshed using an adaptive remeshing algorithm (Zilske et al., 2008) to approx. 18,000 triangles. Both algorithms are natively implemented in Amira®. The final surfaces were exported to the FE software as ASCII .stl-files (STereoLithography).

The final models contained the following separate structures: pars tensa (PT) of the TM, pars flaccida (PF) of the TM, tympano-mallear connection (TMC), malleus, incus, stapes, incudomallear joint (IMJ), incudostapedial joint (ISJ) capsule, ISJ interior, anterior mallear ligament, lateral mallear ligament, posterior incudal ligament, stapedial annular ligament (SAL), tensor tympani (TT) tendon, and stapedius muscle (SM) tendon.

A noteworthy feature of our three geometries is the morphology of the lenticular process of the incus. In all samples, only a thin bony core connected the long process of the incus to the lenticular plate. This core was surrounded by soft tissue, which was labeled as ISJ capsule in our models. A close-up image of this is presented in Figure 1B.

2.3 Finite element analysis

For all FE simulations in this study, Comsol Multiphysics 5.2 (COMSOL AB, Stockholm, Sweden) was used, extended with the Structural Mechanics Module. Once imported into Comsol, the surface models were converted into a tetrahedral volume mesh, to be used in the FE calculation. A mesh refinement study indicated that a surface model of approx. 18,000 triangles, corresponding to a volume mesh containing approx. 120,000 tetrahedral elements, provided an acceptable trade-off

between result accuracy and computation time (the difference in the TF between this mesh and a mesh containing almost twice the number of elements (220,000) was at most frequencies less than 1 dB, and at the most 2.2 dB (around the resonance)). The entire model consists of second-order (quadratic) elements. Using this mesh, most of the TM's interior was adequately meshed using a single layer of quadratic elements, except near the TM's edge. A frequency-domain analysis sweeping over 24 frequencies between 0.1 and 10 kHz took approximately 25 minutes to calculate on a PC (CPU: Intel Xeon E5-2630 v3 @ 2.40 GHz, 8 cores (2 processors installed) – RAM: 128 GB – OS: Windows 7). The 24 frequencies were logarithmically evenly spaced at four frequencies per logarithmic decade below 562 Hz and 16 frequencies per logarithmic decade above 562 Hz.

2.3.1 Boundary conditions of the base models

The following description applies to the base models of this paper and, if not stated otherwise, to all variation models.

The stimulating load on the model was a uniform sound pressure of 1 Pa on the lateral side of the TM. A contiguous selection of triangular faces at the edge of the TM, as well as the end surfaces of the anterior mallear ligament, lateral mallear ligament, posterior incudal ligament, stapedial annular ligament, TT tendon, and stapedius muscle tendon were all fixed. The cochlea was modeled as an acoustic impedance, acting on the medial surface of the stapes footplate (SFP) and the stapedial annular ligament. The value of this impedance was taken from Puria et al. (1997) and is shown in Figure 6B together with data from other sources. Only the amplitude of the cochlear impedance is shown, although the empirical phase from Puria et al. (1997) was incorporated in the model as well. The complex impedance $Z_{\mathrm{ac,\,coch}}$ was implemented as a pressure on the SFP through the expression

$$p_{\mathrm{sfp}} = A_{\mathrm{sfp}} \cdot Z_{\mathrm{ac,\,coch}} \cdot v_{\mathrm{sfp}}, \tag{1}$$

where $A_{\mathrm{sfp}} = 3.08 \cdot 10^{-6} m^2$ (De Greef et al., 2015) is the average footplate area and v_{sfp} is the instantaneous complex stapes velocity normal to the SFP surface.

2.3.2 Material parameters of the base models

All materials except the interior of the ISJ were modelled as solid materials. Most parameter values were adopted from the literature. The Young's moduli of all structures are listed in Table 2.

The PT of the TM was modelled as an orthotropic material within a polar coordinate system with its origin at the umbo. Therefore, the indices i and j in the equations below represent r (radial), c (circumferential), and t (transverse). The transverse direction is approximated by the z-direction of the coordinate system, which is perpendicular to the plane of the tympanic annular ring.

The full stress-strain relation of an orthotropic material in a polar coordinate system is given by:

$$\varepsilon_i = S_{ij}\sigma_j \ , \text{ or} \tag{2}$$

$$\begin{bmatrix} \varepsilon_r \\ \varepsilon_c \\ \varepsilon_t \\ 2\varepsilon_{ct} \\ 2\varepsilon_{tr} \\ 2\varepsilon_{rc} \end{bmatrix} = \begin{bmatrix} \frac{1}{E_r} & -\frac{\nu_{cr}}{E_c} & -\frac{\nu_{tr}}{E_t} & 0 & 0 & 0 \\ -\frac{\nu_{rc}}{E_r} & \frac{1}{E_c} & -\frac{\nu_{tc}}{E_t} & 0 & 0 & 0 \\ -\frac{\nu_{rt}}{E_r} & -\frac{\nu_{ct}}{E_c} & \frac{1}{E_t} & 0 & 0 & 0 \\ 0 & 0 & 0 & \frac{1}{\mu_{ct}} & 0 & 0 \\ 0 & 0 & 0 & 0 & \frac{1}{\mu_{tr}} & 0 \\ 0 & 0 & 0 & 0 & 0 & \frac{1}{\mu_{rc}} \end{bmatrix} \cdot \begin{bmatrix} \sigma_r \\ \sigma_c \\ \sigma_t \\ \tau_{ct} \\ \tau_{tr} \\ \tau_{rc} \end{bmatrix}. \tag{3}$$

Because the symmetry of the compliance matrix S_{ij}, the twelve elasticity parameters (three Young's moduli E_i, six Poisson's ratios ν_{ij}, and three shear moduli μ_{ij}) are reduced to nine independent parameters. In order not to violate the conservation of energy, the strain function energy needs to be positive-definite, placing further restrictions on the Poisson's ratios (Lempriere, 1968).

Li and Barbic (2014) suggested the following simplifications that guarantee the positive-definiteness of the strain energy function, while further reducing the number of tunable parameters from nine to four:

$$\nu_{ij} = \nu\sqrt{\frac{E_i}{E_j}} \ , \text{and} \tag{4}$$

$$\mu_{ij} = \frac{\sqrt{E_i E_j}}{2(1+\nu)}, \tag{5}$$

with $-1 < \nu < 0.5$. Thus, four independent parameters remain to be determined: E_r , E_c , E_t , and ν. The reference value ν for Poisson's ratio was chosen at $\nu = 0.3$. Note that one or even two of the individual Poisson's ratios ν_{ij} can (and in our case, do) have higher values than 0.5 without violating the positive-definiteness of the strain energy function, as long as the third value ensures that their product does not exceed 0.5.

Similar to Tuck-Lee et al. (2008), the radial Young's modulus decreased away from the umbo, emulating the fact that the radially oriented collagen fibers converge at the umbo and manubrium of the malleus, resulting in a higher effective stiffness close to the center. Therefore, the radial Young's modulus was defined by the function

$$E_r(r) = \min\left(40\ \text{MPa} * \frac{2 \cdot 10^{-3}\ \text{m}}{r}, 100\ \text{MPa}\right), \tag{2}$$

so that the value of 40 MPa was reached at $r = 2$ mm from the umbo. In order to avoid divergence when approaching $r = 0$ mm, the function was limited at 100 MPa.Because the radial Young's modulus is non-uniform, the Poisson's ratios and shear moduli that depend on it are non-uniform as well, so they are not characterized by a single value. Three parameters are homogeneous: $\nu_{ct} = 0.6$ (circumferential-transverse), $\nu_{tc} = 0.15$, $\mu_{tc} = 3.85$ MPa.

For the ossicles, no damping was incorporated. For the TM, including pars tensa, pars flaccida, and the tympano-mallear connection, an isotropic loss factor of $\eta = 0.1$ was used (the motivation for this is provided in section 3.2.1). For other soft tissue solid structures, Rayleigh damping with $\alpha = 0\ \text{s}^{-1}$ and $\beta = 10^{-4}$ s was used, equal to some published models (Gan et al., 2002; Liu et al., 2009; Sun et al., 2002).

For all soft tissue structures, the mass density was 1200 kg/m^3 (Homma et al., 2009). The densities of the ossicles were 2390 kg/m^3 (malleus), 2150 kg/m^3 (incus), and 2200 kg/m^3 (stapes) (Homma et al., 2009).

The interior of the ISJ in reality encapsulates articular cartilage on both articular surfaces, synovial fluid, and a meniscus, as modelled in detail by Gan and Wang (2014). However, these components are too small to distinguish the different materials on our µCT images, so as an approximation the entire interior was modeled as a fluid, with a bulk modulus of 2.2 GPa (as used in Zhang and Gan (2011b) and Gan and Wang (2014)) and mass density of 1200 kg/m^3. The physics of the fluid and solid elements were coupled through an acoustic-structure boundary condition in Comsol.

Table 2: List of the Young's moduli of all middle ear structures included in our models.

Structure	Young's modulus (MPa)	Source
Tympanic membrane – pars tensa	$E_r(r)$ (eq. 2) (radial)	Current study
	$E_c = 20$ (circumferential)	Current study
	$E_t = 5$ (z-direction)	Current study
Tympanic membrane – pars flaccida	6.7	$E_c/3$, similar to many sources, see Volandri et al. (2011)
Tympano-mallear connection	2	$E_c/10$, (De Greef et al., 2014a)
Malleus, incus, and stapes	$14.1 \cdot 10^3$	(Cai et al., 2010; Homma et al., 2009)
Incudomallear joint	7	(Homma et al., 2010)
Incudostapedial joint capsule	6	(Koike et al., 2002)
Anterior mallear ligament	21	(Homma et al., 2009)
Lateral mallear ligament	5	(Gan et al., 2004) (6.7 MPa)
Posterior incudal ligament	4.8	(Homma et al., 2009)
Stapedial annular ligament	0.15	Current study*
Tensor tympani tendon	5	(Homma et al., 2010)
Stapedius muscle tendon	0.38	(Homma et al., 2010)

** This value provided a good match with experimental ME response curves and sits well inside the range reported in literature: 0.065 MPa* (Ferrazzini, 2003) *– 5.5 MPa* (Gan et al., 2007).

2.4 Model variations

2.4.1 TM model variations

The effects of quantitative changes to our TM model were examined by changing the TM's Young's modulus and the loss factor (damping). These changes were applied on both PT and PF simultaneously. For the PT, all orthotropic moduli and the maximum value for the radial modulus (i.e. the 100 MPa in equation 6) were scaled by the same factor. The effects of a change in the loss factor of the tympano-mallear connection were calculated as well.

Furthermore, four different material models for the TM were compared. For technical reasons, only the geometries of TB's 1 and 2 were included in this comparison.

- TM model A: isotropic with $E = 20$ MPa and $\nu = 0.3$.
- TM model B: orthotropic with $E_{\mathrm{r}} = 40$ MPa, $E_{\mathrm{c}} = 20$ MPa, and $E_{\mathrm{t}} = 5$ MPa.
- TM model C: non-uniform radial Young's modulus (defined by expression (2). TM model C is used in the base models from this paper.

  TM model D: subdivided TM (Figure 4B). The TM was subdivided in an attempt to represent the arrangement of the collagen fibers even better, similar to Tuck-Lee et al. (2008). The Young's moduli of all sub-regions are orthotropic, but their coordinate systems were different. The inferior region of the TM was identical to TM model C. The superior region was subdivided into three regions, all orthotropic in a Cartesian system. In the region overlying the manubrium of the malleus (indicated by M in Figure 4B), the *y* axis was defined as lying along the manubrium and the *x* axis perpendicular to it. In the anterior and posterior regions, the *x* and *y* axes were rotated 30˚ and -30˚, respectively, and the Young's moduli were $E_{\mathrm{x}} = 40$ MPa and $E_{\mathrm{y}} = 20$ MPa. In the region overlying the manubrium, $E_{\mathrm{x}} = 50$ MPa and $E_{\mathrm{y}} = 10$ MPa, since the radial and circumferential fibers both run more or less along the *x* axis (perpendicular to the manubrium), so that the stiffness in the *x* direction is effectively higher. This microstructural description is largely based on the observations in Lim (1970). In all regions, $E_{\mathrm{z}} = 5$ MPa.

For models B, C, and D, the shear moduli and Poisson's ratios followed the relations in (4) and (5).

2.4.2 Different types of tympano-mallear connection

As reported by De Greef et al. (2016), the anterior-posterior width of the tympano-mallear connection (TMC) varies over an order of magnitude among individuals: in the narrowest TMC sample the minimal width was 83 ± 7 μm, while in another sample the TMC was 840 ± 7 μm at its narrowest point. Yet all samples exhibited a very similar TMC near the umbo and near the lateral process of the malleus: at both locations, the connection between TM and malleus was wide and tight.

In order to evaluate the influence of the different types of TMC, two models were compared with identical geometry for the entire ME, except for the TMC. To do this, we started from a sample

with a narrow TMC by nature (sample 1) and adapted it so that the TM was more tightly connected to the manubrium, similar to the most tight connection reported in De Greef et al. (2016). To do this, we started from the segmentation masks of sample 1 in Amira®, deleted the mask of the TMC and rotated the TM mask towards the manubrium around the anterior-posterior axis through the umbo, so that the distance between TM and malleus decreased. After this, the segmentation of the TM was adapted near the manubrium so that it touches the manubrium along its entire length. In this wide-TMC model, there was no separate material anymore for the TMC, because the microstructural observations in De Greef et al. (2016) demonstrated that in those cases, the TM is directly connected to the malleus without a distinct connection structure. One cross-section of this segmentation is visible in Figure 5B. After this, the masks were triangulated and imported into Comsol in the same way as the other geometries. Then, the same material parameters and boundary conditions were assigned to this geometry and the simulation was run for the same frequencies. The results from this simulation could then be compared to the results from the simulations with the original geometry.

2.4.3 Other ME/IE model variations

The effects of quantitative changes in cochlear impedance (by comparing the complex impedances from different literature sources), the Young's moduli of multiple materials, and the Rayleigh damping coefficients of soft tissue (outside the TM) were determined. Finally, the influences of the length of the tensor tympani tendon and of the material model for the incudostapedial joint interior (fluid vs. solid) were studied.

3 Results

3.1 Base models

Figure 1 illustrates our three FE models, based on three different geometries, together with a close-up of the ISJ of geometry 1.

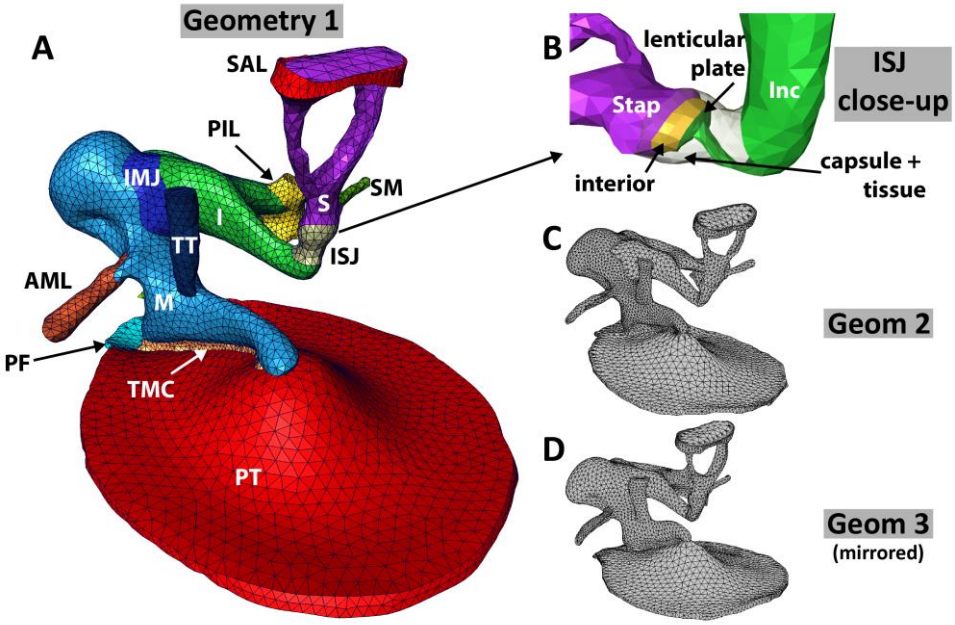

Figure 1: A: A detailed screenshot of the surface model of sample 1. B: close-up image of the ISJ (geometry 1). The ISJ interior is modeled as a fluid, the rest of the model as a solid. C & D: geometries 2 and 3.

Figure 2A presents the piston component of the SFP velocity amplitude in our three geometries as a function of frequency. The figure also shows a summary of experimental data as presented by Rosowski et al. (2007), consisting of a grand mean of mean curves from multiple independent studies and twice the standard deviation of those means. Between 100 Hz and 750 Hz, the average slope of the model curves is +6.5 dB/octave, similar to the slope of +5.7 dB/octave in the average experimental curve. The first resonance peaks are all near 1 kHz and the average slope between 1.5 and 10 kHz is -8.2 dB/octave in the model and -6.1 dB/octave in the experiments. However, after the peak, the curves of the individual geometries are clearly less smooth than the experimental average and a significant second maximum occurs in all three geometries between 2 and 4 kHz. Therefore, it is valuable to compare the individual model results to individual experimental curves, in contrast to a grand mean of many individuals. Figure 2B presents such curves (reported in Aibara et al. (2001)) and indeed shows more intra-specimen variability in the frequency dimension than the average does. The curves were rescaled by a factor of $1/\sqrt{2}$ compared to the published values to correct for a difference in the normalization. The data in Aibara et al. (2001) were normalized to 1 Pa RMS, whereas our data and

those from Rosowski et al (2007) were normalized to 1 Pa peak amplitude (confirmed in personal communication by K.N O'Connor on June 29th 2016).

Figure 2C shows the average response of our three models, indicating that averaging over more samples indeed smooths the response curve and improves similarity to the experimental average, especially above 2 kHz.

Figure 2D presents the phase of the SFP TF and shows approximate agreement with experimental average data from Aibara et al. (2001) (no average TF phase was reported in Rosowski et al. (2007)).

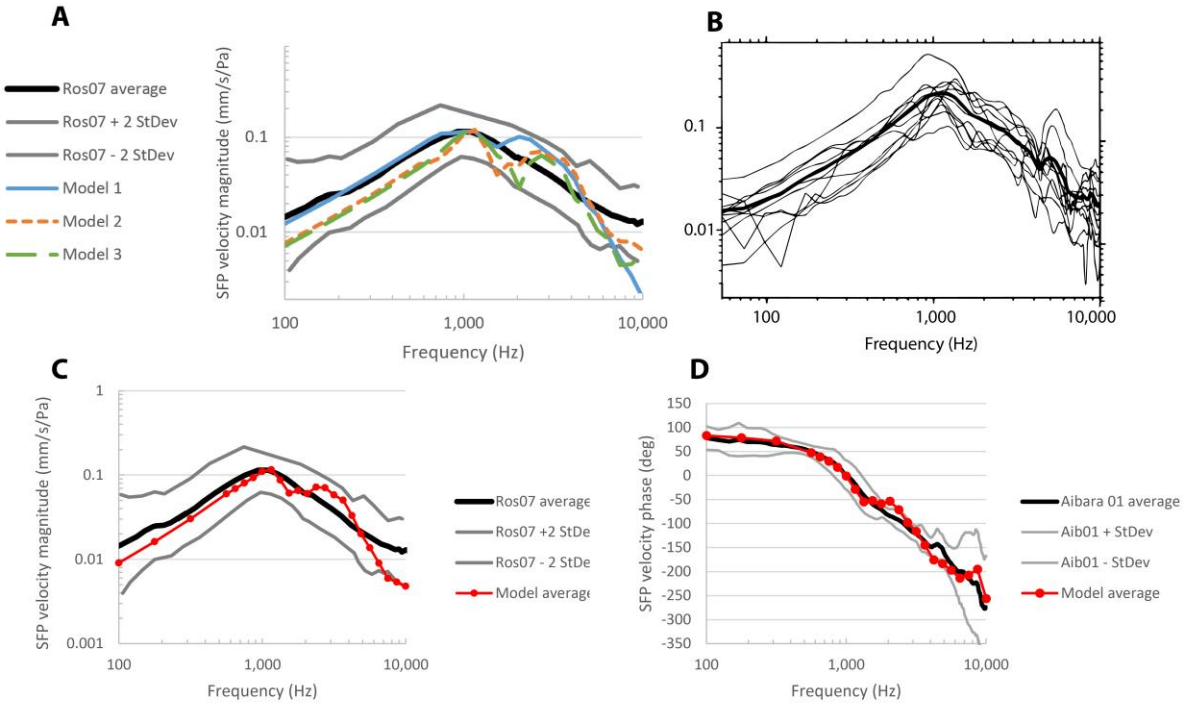

Figure 2. A:. Stapes velocity TF of our three geometries, compared to the experimental average from Rosowski et al. (2007) – B: Individual experimental curves of the stapes velocity TF, adapted from Aibara et al. (2001) – C: Average stapes response curve for our three geometries, compared to the average experimental curve from Rosowski et al. (2007) – D: Average phase of the SFP TF relative to the phase of the pressure on the TM for our three models and average experimental data from Aibara et al. (2001).

3.2 Tympanic membrane variations

3.2.1 TM damping

Figure 3A demonstrates the influence of TM damping on the stapes velocity TF. It shows the average TF of the base models and of models with a higher and lower constant loss factor (η) in the TM. The largest changes occur around 3 kHz, i.e. around the second TF maximum, and at 10 kHz. The maximal differences around 3 kHz are +2.0 dB ($\eta = 0.02$) and -3.4 dB ($\eta = 0.5$), and at 10 kHz +2.3 dB ($\eta = 0.02$) and -3.9 dB ($\eta = 0.5$). Increasing the damping smooths the response curve, making it more similar to the average experimental curve. However, it makes the individual response curves unrealistic, compared to the individual experimental curves from Aibara (2001) (see Figure 2B).

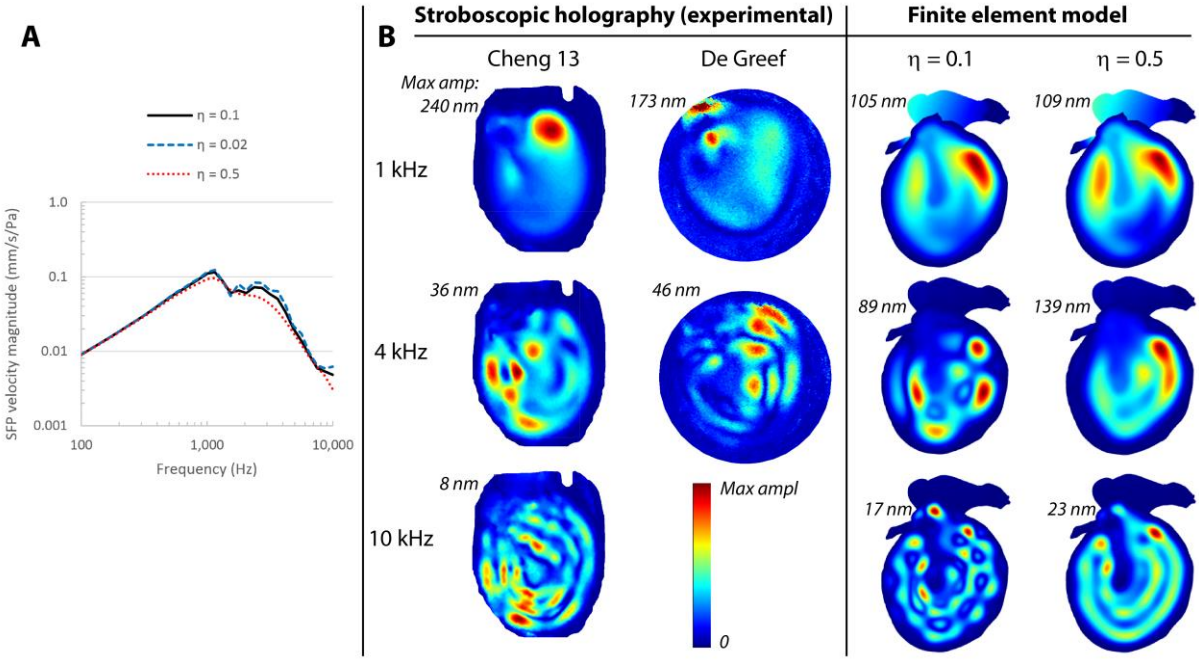

Figure 3. A: Influence of TM damping variation on the average SFP TF. η = 0.1 represents the base models. The curves represent averages over our three geometries ; B: Vibration magnitude patterns of the TM, determined experimentally (Cheng et al., 2013; De Greef et al., 2014b) *and through our FE model (geometry 1), using two different loss factors. The dataset from De Greef is limited to 6.4 kHz, so no data at 10 kHz is available. The maximum amplitudes for each dataset are mentioned next to the patterns. The displacements are normalized to 1 Pa sound pressure. The color bar is shared by all datasets, but the ranges differ (depending on the maximum amplitude of each dataset).*

Furthermore, a comparison of the measured full field vibrational patterns of the tympanic membrane to the calculated patterns in the model (Figure 3B) indicates that the match is worse for

the model with high damping than for the base model. The higher damping model produces patterns that are too smooth in the spatial domain, compared to the experimental observations. The column titled 'De Greef' presents data that has not been published before and that was recorded using the setup for stroboscopic holography at our lab, described in De Greef et al. (2014b).

3.2.2 TM material model: isotropic, orthotropic, non-uniform, and subdivided

Figure 4A depicts the difference in SFP velocity for the four different material models of the TM as described in section 2.4. None of the other models deviates more than 3.3 dB from the base model. Figure 4B provides an illustration of the coordinate systems in the subdivided TM model (model D). Figure 4C presents TM vibration magnitude patterns of the four different TM models at stimulation frequencies of 1 kHz, 4.2 kHz, and 10 kHz. The patterns as well as the maximum vibration amplitude are very similar for the different TM models.

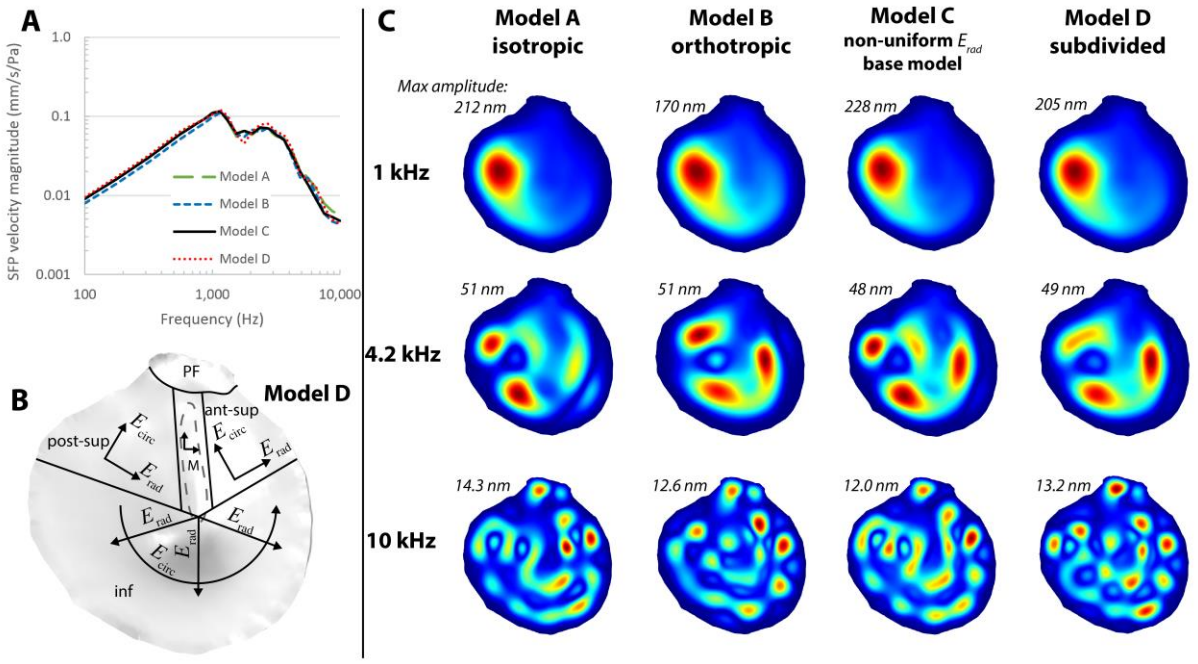

Figure 4: A: Influence of TM material models on the average SFP TF from the models based on geometries 1 and 2. Model A: Isotropic - Model B: Orthotropic - Model C: Orthotropic with decreasing E_{rad} - Model D: Subdivided TM (depicted in subfigure B). B: Subdivided TM model (model D). C: TM vibration magnitude patterns for the four models at three frequencies for the FE model based on geometry 2. The maximum amplitudes for each model and frequency are mentioned next to the patterns.

3.2.3 Tympano-mallear connection

The effects of the width and type of tympano-mallear connection (TMC) are illustrated in Figure 5A. Figure 5B and C illustrate the difference between the wide and narrow TMC geometry halfway along the manubrium. The change in SFP velocity is less than 2.3 dB over the entire frequency range.

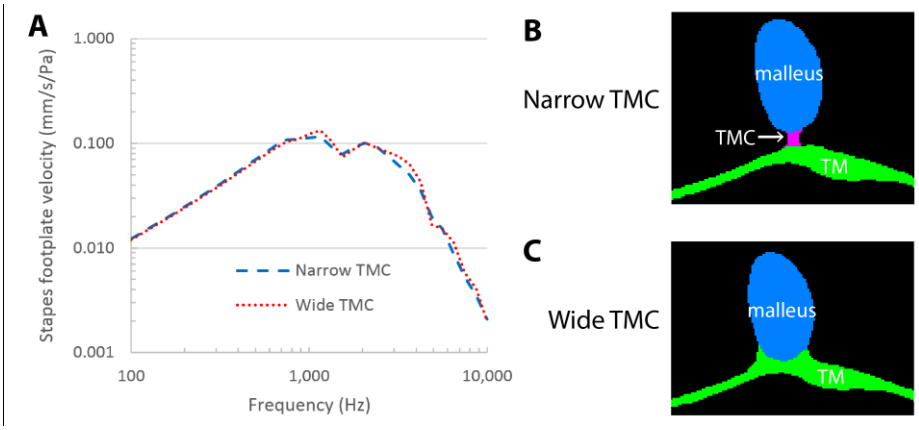

Figure 5. A: Impact of the width of the tympano-mallear connection (TMC) on middle ear transmission of the model, based on geometry 1. B & C: Segmented masks representing the malleus, TMC, and TM for the narrow TMC (B) and wide TMC (C) models. In the wide TMC model, the TMC is actually absent and the TM is directly attached to the malleus along the entire manubrium.

3.3 Cochlear impedance

Figure 6A shows the model responses when using cochlear impedance data from four different previous studies, averaged over our three geometries in each case and keeping all other parameters equal. The model incorporating the impedance from Puria et al. (1997) is our base model and produces a less distinct second peak in the 2-4 kHz range than the other models. Its cochlear impedance has a more positive slope at frequencies above 1 kHz, as shown in Figure 6B.

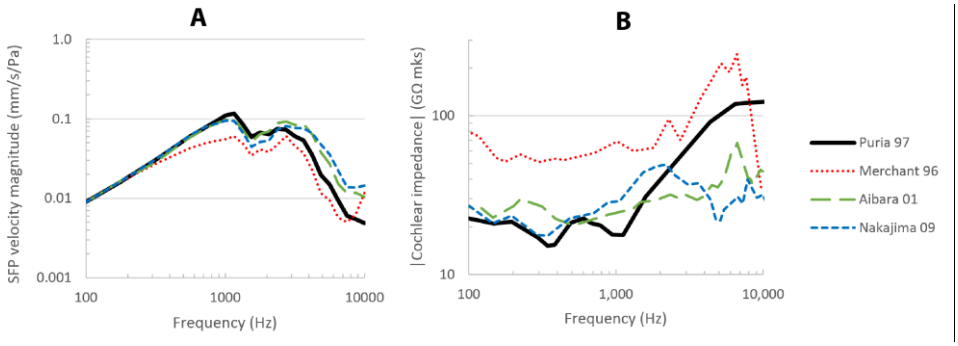

Figure 6: A: Effects of the incorporation of cochlear impedance data from different studies on the stapes velocity TF (Aibara et al., 2001; Merchant et al., 1996; Nakajima et al., 2009; Puria et al., 1997). *The curves represent averages over*

our three geometries. B: Comparison of the different literature sources for the magnitude of the acoustic impedance of the cochlea. The legend is the same for both plots. The impedance data from Aibara et al. (2001) *was rescaled by a factor of* $\sqrt{2}$ *compared to the published values to correct for an error in their calculation of the impedance: there was inconsistency between the velocity and pressure calibrations (the former in peak units and the latter in RMS units) (confirmed in personal communication by K.N O'Connor on August 25th 2016).*

3.4 Other quantitative variations

In Figure 7, the effects of other quantitative changes in the model are presented. All variations consist of a multiplication and division by 5 of a single material parameter, keeping all other parameters constant. All plotted curves represent the average response over the three geometries.

Increasing the Young's modulus of the TM shifted the first and second peaks to higher frequencies and decreased the second/first peak ratio from 1.1 (E_{TM}/5) to 0.62 (base model) and finally 0.58 (E_{TM}x5) (Figure 7A). The influence (in absolute value) of the Young's moduli of the TMC and stapedius muscle (Figure 7B and G), and the loss factor of the TMC (Figure 7H) was nowhere larger than 1.05 dB. Decreasing and increasing the Young's modulus of the ISJ capsule had an effect of 3.8 dB and 1.8 dB at the most, respectively (Figure 7D).

The influence of the Young's modulus of the stapedial annular ligament (Figure 7C) is largest at frequencies below 1 kHz with changes of at least +4 dB (E_{SAL}/5) and -10 dB (E_{SAL}x5). However, above 2.1 kHz the influence is never larger than +2 dB (E_{SAL}/5) and -5 dB (E_{SAL}x5).

The Young's modulus of the IMJ (Figure 7E) has influence over the entire frequency range, with the smaller option (E_{IMJ}/5) producing a response change of up to -7.7 dB, while the larger option (E_{IMJ}x5) results in a change of up to +3.5 dB. While a decrease in TT's stiffness (Figure 7F) produces a change of +1.6 dB at most, an increase has an influence of up to -4.8 dB (at 1 kHz). Finally, the β-coefficient of Rayleigh damping (Figure 7I), applied to all ME soft tissues except the TM, had an influence around the resonance of up to +6 dB for β/5 and -9 dB for βx5.

Varying the Poisson's ratio (i.e. the value of ν in eq. (4)) from 0.3 to 0.49 or 0.1 changed the SFP velocity magnitude by less than 2 dB for all frequencies in both scenarios (no graph shown).

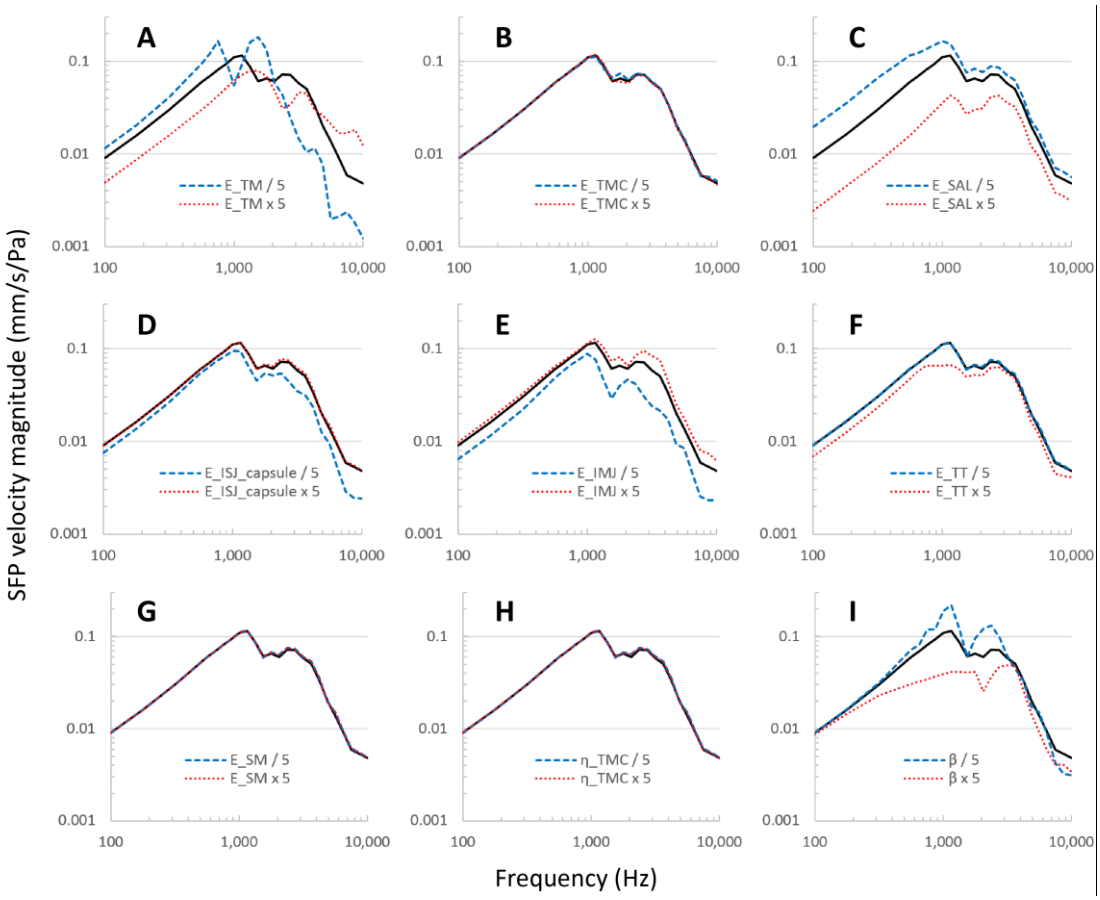

Figure 7: Influence of different variations in material parameters. All curves represent average responses over our three geometries. E: Young's modulus – β: Rayleigh damping paramater of soft tissue structures except TM – η: Loss factor.

3.5 Qualitative changes to the ME model

3.5.1 Incudostapedial joint microstructure

In our base model, the ISJ is modelled as a fluid pocket within a solid capsule. This joint model is compared to a fully solid joint model in Figure 8A. The motivation for this comparison is discussed in section 4.5.1. In the case of a fully solid joint, three scenarios are compared in which the Young's modulus of both the ISJ interior and the ISJ capsule were changed: 0.6 MPa (as in Prendergast et al. (1999) and Gan et al. (2004)), 6 MPa (as in Cai et al. (2010)), and 60 MPa (for consistency). For the solid model with $E = 0.6$ MPa, the response change compared to the base fluid model ranges from -0.8 dB to -2.7 dB below 2.5 kHz and -3.0 dB to -6.7 dB above 2.5 kHz, while for the solid model with, $E = 6$ MPa, it differs by at most 0.9 dB from the fluid model. Increasing the Young's modulus further to 60

MPa increased the differences again, so that they are up to 2.2 dB (at 8.7 kHz), but still smaller than 1 dB below 3 kHz.

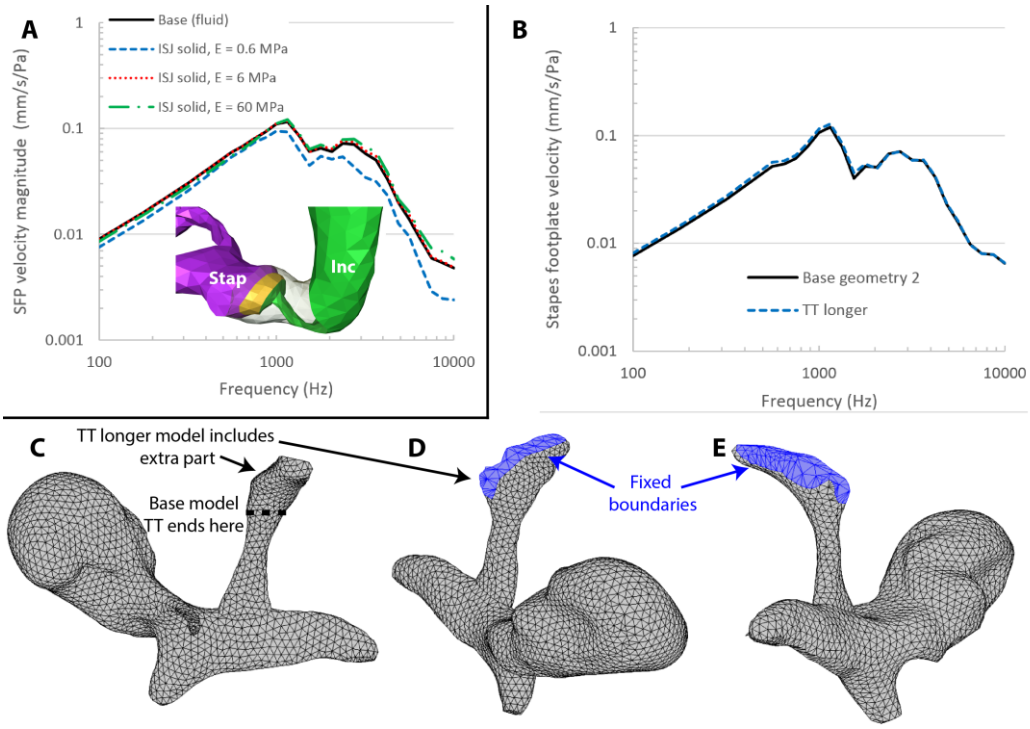

Figure 8: A: Influence of modeling the ISJ interior as a fluid or solid, for two different Young's moduli of both ISJ interior and capsule in the case of the solid model. Note that the red dotted line and the black base curve differ only by nature of the ISJ: solid or fluid. All curves represent the average responses for our three geometries. B: Influence of the length of the tensor tympani tendon on ME transmission of the model based on geometry 2. Note that the two curves almost overlap. C: Illustration of the lengths of the TT geometry in the base model and the model with a longer TT. The dashed line indicates where the TT tendon terminates in the base models of all three geometries. D&E: views from the postero-superior (D) and postero-inferior (E) side of the malleus of the model with a longer TT. Blue surfaces indicate fixed boundary conditions (only boundary conditions at the tendon are shown).

3.5.2 Tensor tympani tendon length

As can be seen in Figure 1, the base models contain only a portion of the tensor tympani tendon. An alternative model was constructed for geometry 2, in which a larger part of the tendon was included (see Figure 8C, D, and E). The motivation for this comparison is presented in section 4.5.2. Figure 8B (blue curve) shows that the influence of this change is smaller than 1 dB over the entire frequency range, and for this reason, the additional effort of including the longer TT tendon model was not made

for the other geometries. For the sake of consistency, the shorter TT tendon version was used in the final model of geometry 2 as well.

4 Discussion

4.1 Model validation

The agreement between the model results and reported experimental results can be judged from Figure 2 and Figure 3. The largest discrepancy between our modeling results and reported average experimental ME response curves is the local maximum in our models between 2-4 kHz. The peak is present in all three geometries, but has a larger relative height with respect to the first resonance in geometry 1 than in the other two (see Figure 2A).

Since the models represent individual ears, they should each result in the response of an individual measurement, not the average response in which variations in the frequency domain are smoothed due to the averaging (see Figure 2). If an attempt is made to match the response of a ME model based on a single geometry to the average experimental response, the risk exists that unrealistic material parameters need to be applied, as discussed in the next section on TM damping. On the other hand, when applying the same set of parameters to different geometries, the average result should approach the average experimental result as the number of tested geometries increases and this would be a fine confirmation of the correctness of the parameters. Since constructing additional models based on different geometries is labor intensive, the number was limited to three in this paper. Nevertheless, the average model response presented in Figure 2C suggests that the currently used parameter set is adequate for middle ear modeling within the context of linear simulations in the frequency range 0.1 – 10 kHz, with some reservations between 2 and 4 kHz, where all three models differ from the experimental data.

4.2 TM damping

Figure 3 shows that one possible parameter change that has enough influence to reduce the discrepancy between model and experiment at 2-4 kHz is an increase in TM damping. Many published

ME models employ Rayleigh damping in the TM, with coefficients $\alpha = 0\ \mathrm{s}^{-1}$, $\beta = 0.75 \cdot 10^{-4}$ s (Gan et al., 2006, 2004), or $\alpha = 0\ \mathrm{s}^{-1}$, $\beta = 1 \cdot 10^{-4}$ s (Liu et al., 2009; Sun et al., 2002). In the case of $\beta = 0.75 \cdot 10^{-4}$ s, converted through $\eta = \frac{\alpha}{\omega} + \beta\omega$, this corresponds to $\eta = 0.047$ at 100 Hz, $\eta = 0.47$ at 1 kHz, and $\eta = 4.7$ at 10 kHz, i.e. higher than $\eta = 0.5$ at most frequencies above 1 kHz. However, the results presented in Figure 3 strongly suggest that a loss factor of $\eta = 0.5$ (and consequently, higher values as well) results in unrealistic TM vibration patterns that are overdamped and exhibit too few local maxima. Very similar behavior was observed in the model of De Greef et al. (2014a) that was focused on (and consisted of only) the TM and the malleus. It should be noted that the frequency spacing used in this paper is rather coarse compared to the fine structure of the TF in the high frequency range (> 4 kHz) (see Figure 2B), which limits the reliability of conclusions about damping in this range.

4.3 Cochlear impedance

The incorporated cochlear impedance obviously has a profound influence on the motion of the stapes footplate. Therefore, the choice of the values used for this impedance has a large influence on the ME TF. The reported sources for cochlear impedances (see Figure 6) determined the impedance values through differing methods and show large mutual differences. The discussed 2-4 kHz discrepancy between our models and experimental TF's was smallest when implementing the data from Puria et al. (1997). Nakajima et al. (2009) highlighted the difficulties of experimentally determining the cochlear impedance at frequencies above 1 kHz, since in that range the stapes motion becomes multi-dimensional and the full 3D motion of the stapes should be determined. Therefore, additional experimental data on this will be very useful, and for now the dataset was implemented that produced results with the smallest deviation from experimental ME TF's, i.e. the cochlear impedance from Puria et al. (1997), even though it is not the most recent source.

4.4 Other TM model variations

The results in Figure 4 demonstrate that the different degrees of sophistication of the TM material model explored in this study lead to differences of less than 3.3 dB over the frequency range 0.1 – 10 kHz. In addition to this, the vibration patterns of the TM also did not change in a fundamental way when applying the different TM models. These conclusions are contradictory to the conclusions posed in Fay et al. (2006) and Tuck-Lee et al. (2008), but these papers studied feline (as opposed to human) middle ear models with different modeling approaches and parameter values. However, our results suggest that for linear modeling of an intact, non-pathological middle ear in the auditory frequency spectrum, a simple isotropic TM model could be as appropriate as a more sophisticated model.

The Young's modulus of the TM has a very strong influence on ME transmission, as observed in Figure 7A. This is expected and similar to findings of other studies, e.g Hoffstetter et al. (2010) and Maftoon et al. (2015).

The influence of the type of tympano-mallear connection (narrow or wide) was limited to 2.3 dB (see Figure 5). In both models, the connection was tight at the umbo and lateral process of the malleus and how tight the connection is in between these two ends appears to be almost irrelevant. However, this is currently only confirmed within the limits of this study, i.e. an intact, non-pathological middle ear model in the linear, auditory regime. Furthermore, it should be noted that, in order to construct the wide TMC model, the angle between the TM and the rest of the model needed to be changed. This could have a separate effect on ME transmission that confounds the results. Koike et al. (2002) also performed a comparison of FE models with tight and loose TMC's and concluded that "*the modification of the attachment between the malleus handle and the tympanic membrane did not greatly influence the vibration mode and displacement of the tympanic membrane*".

Finally, the studied variation in TMC loss factor introduced a maximal difference of 0.8 dB (Figure 7H), i.e. a negligible influence.

4.5 Qualitative changes to the ME model

The two reported qualitative changes to the ME models were chosen on the basis of the hypothesis that they could reduce the peak between 2-4 kHz in the TF and thereby improve the match with experimental ME TF's, as discussed in the following sections.

4.5.1 Incudostapedial joint microstructure

A previous version of our model included a solid ISJ interior with a Young's modulus of 0.6 MPa. Upon inspecting the different subsystems in our ME models (TM, incudomallear complex, and stapes), the stapes featured the highest resonance frequency, between 3-5 kHz (results not shown). Therefore, the hypothesis was formulated that if the stapes motion were coupled more strongly to the motion of the much heavier incudomallear complex (their mass ratio is approximately 20 to 1 (De Greef et al., 2015)), the free motion of the stapes and therefore also the resonance mode at the 'problematic' frequencies would be suppressed.

As can be seen in Figure 8A, increasing the Young's modulus to 6 MPa did change the overall stapes velocity, but replacing the interior with a fluid did not alter the ME response further for our model. The ME model by Gan and Wang (2014) contained more microstructural details in the ISJ, such as articular cartilage and a meniscus, and their results suggested that modeling the synovial nature of the joint improves the match with experimental data and is therefore influential for ME transmission. Other dedicated studies on modeling the ISJ, including Funnell et al. (2005) and (2006) and Zhang et al. (2011b), also included more microstructural details than our model, but were restricted to low frequency stimulations (not further specified). Further focused study is needed to make final conclusions about the role of ISJ microstructure in sound transmission of the human ME.

4.5.2 Tensor tympani tendon length

Since the 2-4 kHz peak is situated at frequencies higher than the system's first resonance (around 1 kHz), another hypothesis was that it is caused by the absence of a mass in our model that is present in real TB's. The rationale behind this was that the mechanical response of a system is dominated by inertia, i.e. by mass, at frequencies above its resonance. One candidate is the tensor tympani tendon,

a relatively bulky structure compared to other ME muscles and tendons, that was only partly included in our base model. The results presented in Figure 8B show that incorporating a significantly larger portion of the TT tendon only alters the model's response by less than 1 dB in the frequency range 0.1 - 10 kHz. Because of this small influence, because the entire TT was difficult to segment, and because the definition of boundary conditions is ambiguous when the entire tendon and muscle are included, only a portion of the TT tendon was included in our final model.

4.6 Comparison to other studies and limitations of the current study

Already in 1978, researchers were investigating the influence of parameter variation in FE models of the ME (Funnell and Laszlo, 1978). More recently, Hoffstetter et al. (2010) published an extensive study of which the design was very similar to the current paper: after constructing a FE model of the human ME, based on realistic geometry, many different parameters and model features were varied and their influences on the stapes footplate transfer function were evaluated.

For the TM damping, similar results to ours were reported: the influence is modest and only notable between 1-4 kHz, i.e. around and above the resonance frequency. Outside of this range, a change of 25% in material damping had an effect of less than 5% (Hoffstetter et al., 2010).

For the TMC, contradictory results were reported – they found a large influence (> 25% change) when excluding or including the TMC (named stria mallearis there), although their approach to modeling and varying the TMC was different from ours and the results are therefore difficult to compare.

Hoffstetter et al. (2010) varied only the mass of the cochlear fluid, not other components of the acoustical impedance, and found that changing it by 50% had a negligible (<5%) effect on ME transmission for all simulated frequencies. They found that varying the TM's stiffness had a very large influence above 500 Hz, but almost none below it. This latter observation is contradictory to our results. Another significant difference between the conclusions is that they reported a negligible influence (5%) of the stapedial annular ligament, compared to a very large influence observed through our models. They found that the IS and IM joints had comparable, large influences, in contrast to our

results that suggest that only the IM joint's parameters are very influential. Their observation regarding the effect of the stiffness of both middle ear muscles was on the other hand similar to ours.

It should be mentioned that one limitation of the current study is the variation of just a single parameter at a time. In complex mechanical systems such as the ME, parameter influences can be coupled, i.e. the effect of changing parameter A could be different for different values of parameter B. These coupled effects are not detected using the current method. In the interpretation of the results it is important to keep this methodological limitation in mind.

At this point we also need to rectify two errors in a previous paper by the same first author (De Greef et al., 2015). In that paper, the bending theory of the pedicle of the lenticular process of the incus was mentioned (Funnell et al., 2005). Funnell et al. proposed the possibility that the thin pedicle may bend during ossicular motion in certain vibration modes (especially at higher frequencies), "thereby adding flexibility to the [incudostapedial joint] and reducing the transmission of particular motion components from the incus to the stapes". In the paper by De Greef et al., it was stated that if the pedicle consists of bone instead of strongly calcified cartilage (which are not distinguishable from each other on micro-CT images but have a different Young's modulus by approximately a factor of 10), the 'bending theory' would be undermined. However, Funnell et al. did indeed propose bending in a full bony pedicle, not only a cartilaginous one. Furthermore, the paper by Decraemer and Khanna (2004) was cited to mention bending in the pedicle of the lenticular process as well, but the concept is not covered by Decraemer and Khanna.

5 Conclusions

This study aimed to examine the influence of various quantitative and qualitative variations in parameter values and model definitions on sound transmission in human ME FE models. The most important quantitative parameters were found to be the Young's moduli of the tympanic membrane (TM), the stapedial annular ligament, the incudomallear joint, and the tensor tympani, the loss factor of the TM, the β Rayleigh damping coefficients for the soft tissues outside the TM, and the choice of

545 cochlear impedance. Less influential parameters were the Young's moduli of the tympano-mallear connection, incudomallear joint capsule, and stapedius muscle, and the loss factor of the tympano-mallear connection.

The inclusion of multiple individual geometries in a single FE study allowed the calculation of an average stapes velocity response function, and confirmed that this matches experimental average 550 response curves better than individual models. The largest discrepancy appeared in the 2-4 kHz range, where the model response was higher than the average experimental result. Due to the wide variation in experimental response curves of individuals, the average outcome of the models falls within the standard deviation observed for individual temporal bones at most frequencies.

Acknowledgements

555 The first two authors of this paper are funded by the Flanders Research Foundation (FWO).

References

Aibara, R., Welsh, J.T., Puria, S., Goode, R.L., 2001. Human middle-ear sound transfer function and cochlear input impedance. Hear. Res. 152, 100–109. doi:10.1016/S0378-5955(00)00240-9

Buytaert, J., Goyens, J., De Greef, D., Aerts, P., Dirckx, J., 2014. Volume Shrinkage of Bone, Brain and Muscle Tissue in Sample Preparation for Micro-CT and Light Sheet Fluorescence Microscopy (LSFM). Microsc. Microanal. 20, 1208–1217. doi:10.1017/S1431927614001329

Cai, H., Jackson, R.P., Steele, C.R., Puria, S., 2010. A Biological Gear in the Human Middle Ear, in: Proceedings of the COMSOL Conference 2010.

Cheng, J.T., Hamade, M., Merchant, S.N., Rosowski, J.J., Harrington, E., Furlong, C., 2013. Wave motion on the surface of the human tympanic membrane: holographic measurement and modeling analysis. J. Acoust. Soc. Am. 133, 918–37. doi:10.1121/1.4773263

De Greef, D., Aernouts, J., Aerts, J., Cheng, J.T., Horwitz, R., Rosowski, J.J., Dirckx, J.J.J., 2014a. Viscoelastic properties of the human tympanic membrane studied with stroboscopic holography and finite element modeling. Hear. Res. 312, 69–80. doi:10.1016/j.heares.2014.03.002

De Greef, D., Buytaert, J.A.N., Aerts, J.R.M., Van Hoorebeke, L., Dierick, M., Dirckx, J., 2015. Details of human middle ear morphology based on micro-CT imaging of phosphotungstic acid stained samples. J. Morphol. 276, 1025–46. doi:10.1002/jmor.20392

De Greef, D., Goyens, J., Pintelon, I., Bogers, J.-P., Van Rompaey, V., Hamans, E., Van de Heyning, P., Dirckx, J.J.J., 2016. On the connection between the tympanic membrane and the malleus. Hear. Res. 340, 50–59. doi:10.1016/j.heares.2015.12.002

De Greef, D., Soons, J., Dirckx, J.J.J., 2014b. Digital Stroboscopic Holography Setup for Deformation Measurement at Both Quasi-Static and Acoustic Frequencies. Int. J. Optomechatronics 8, 275–291. doi:10.1080/15599612.2014.942928

Decraemer, W.F., Khanna, S., 2004. Measurement, visualization and quantitative analysis of complete three-dimensional kinematical data sets of human and cat middle ear, in: Wada, H. (Ed.), Proceedings of the 3rd Symposium on Middle Ear Mechanics in Research and Otology. World Scientific, Singapore, pp. 3–10.

Fay, J.P.J.P., Puria, S., Steele, C.R., 2006. The discordant eardrum. Proc. Natl. Acad. Sci. U. S. A. 103, 19743–19748. doi:10.1073/pnas.0603898104

Ferrazzini, M., 2003. Virtual middle ear A dynamic mathematical model based on the finite element method. Swiss Federal Institute of Technology.

Funnell, W.R.J., Daniel, S.J., Alsabah, B., Liu, H., 2006. On the coupling between the incus and the stapes, in: Ninth “Mechanics of Hearing” Workshop. Portland, p. 22.

Funnell, W.R.J., Heng Siah, T., McKee, M.D., Daniel, S.J., Decraemer, W.F., 2005. On the coupling between the incus and the stapes in the cat. J. Assoc. Res. Otolaryngol. 6, 9–18. doi:10.1007/s10162-004-5016-3

Funnell, W.R.J., Laszlo, C.A., 1978. Modeling of the cat eardrum as a thin shell using the method. J. Acoust. Soc. Am 63, 1461–1467.

Gan, R.Z., Feng, B., Sun, Q., 2004. Three-dimensional finite element modeling of human ear for sound transmission. Ann. Biomed. Eng. 32, 847–59.

Gan, R.Z., Reeves, B.P., Wang, X., 2007. Modeling of sound transmission from ear canal to cochlea.

Ann. Biomed. Eng. 35, 2180–2195. doi:10.1007/s10439-007-9366-y

Gan, R.Z., Sun, Q., Dyer, R.K., Chang, K.-H., Dormer, K.J., 2002. Three-dimensional Modeling of Middle Ear Biomechanics and Its Applications. Otol. Neurotol. 23, 271–280. doi:10.1097/00129492-200205000-00008

Gan, R.Z., Sun, Q., Feng, B., Wood, M.W., 2006. Acoustic-structural coupled finite element analysis for sound transmission in human ear--pressure distributions. Med. Eng. Phys. 28, 395–404. doi:10.1016/j.medengphy.2005.07.018

Gan, R.Z., Wang, X., 2014. Modeling Microstructure of Incudostapedial Joint and the Effect on Cochlear Input Finite Element Modeling of ISJ Microstructure, in: Mechanics of Hearing Proceedings. Cape Sounio.

Gentil, F., Garbe, C., Parente, M., Martins, P., Ferreira, A., Jorge, R.N., Santos, C., Paço, J., 2014. Analysis of Eardrum Pathologies Using the Finite Element Method. J. Mech. Med. Biol. 14, 1450034. doi:10.1142/S0219519414500341

Hege, H., Seebass, M., Stalling, D., Zockler, M., 1997. A Generalized Marching Cubes Algorithm Based On Non-Binary Classifications. ZIB Prepr. sc-97-05.

Hoffstetter, M., Schardt, F., Lenarz, T., Wacker, S., Wintermantel, E., 2010. Parameter study on a finite element model of the middle ear. Biomed. Eng. (NY). 55, 19–26. doi:10.1515/BMT.2010.006

Homma, K., Du, Y., Shimizu, Y., Puria, S., 2009. Ossicular resonance modes of the human middle ear for bone and air conduction. J. Acoust. Soc. Am. 125, 968–79. doi:10.1121/1.3056564

Homma, K., Shimizu, Y., Kim, N., Du, Y., Puria, S., 2010. Effects of ear-canal pressurization on middle-ear bone- and air-conduction responses. Hear. Res. 263, 204–15. doi:10.1016/j.heares.2009.11.013

Koike, T., Wada, H., Kobayashi, T., 2002. Modeling of the human middle ear using the finite-element method. J. Acoust. Soc. Am. 111, 1306–1317. doi:10.1121/1.1451073

Lempriere, B.M., 1968. Poisson's ratio in orthotropic materials. AIAA J. 6, 2226–2227. doi:10.2514/3.4974

Li, Y., Barbic, J., 2014. Stable Orthotropic Materials, in: Proceedings of the 2014 ACM SIGGRAPH/Eurographics Symposium on Computer Animation.

Lim, D.J., 1970. Human Tympanic Membrane: An Ultrastructural Observation. Acta Otolaryngol 70, 176–186.

Liu, Y., Li, S., Sun, X., 2009. Numerical analysis of ossicular chain lesion of human ear. Acta Mech. Sin. Xuebao 25, 241–247. doi:10.1007/s10409-008-0206-6

Maftoon, N., Funnell, W.R.J., Daniel, S.J., Decraemer, W.F., 2015. Finite-Element Modelling of the Response of the Gerbil Middle Ear to Sound. JARO - J. Assoc. Res. Otolaryngol. 16, 547–567. doi:10.1007/s10162-015-0531-y

Masschaele, B.C., Cnudde, V., Dierick, M., Jacobs, P., Van Hoorebeke, L., Vlassenbroeck, J., 2007. UGCT: New X-ray radiography and tomography facility. Nucl. Instruments Methods Phys. Res. Sect. A Accel. Spectrometers, Detect. Assoc. Equip. 580, 266–269. doi:10.1016/j.nima.2007.05.099

Merchant, S.N., Ravicz, M.E., Rosowski, J.J., 1996. Acoustic input impedance of the stapes and cochlea in human temporal bones. Hear. Res. 97, 30–45.

Nakajima, H.H., Dong, W., Olson, E.S., Merchant, S.N., Ravicz, M.E., Rosowski, J.J., 2009. Differential intracochlear sound pressure measurements in normal human temporal bones. JARO - J. Assoc.

Res. Otolaryngol. 10, 23–36. doi:10.1007/s10162-008-0150-y

Prendergast, P.J., Ferris, P., Rice, H.J., Blayney, A.W., 1999. Vibro-Acoustic Modelling of the Outer and Middle Ear Using the Finite-Element Method. Audiol. Neuro-Otology 4, 185–191. doi:10.1159/000013839

Puria, S., Peake, W.T., Rosowski, J.J., 1997. Sound-pressure measurements in the cochlear vestibule of human-cadaver ears. J. Acoust. Soc. Am. 101, 2754–2770. doi:10.1121/1.418563

Rosowski, J.J., Chien, W., Ravicz, M.E., Merchant, S.N., 2007. Testing a method for quantifying the output of implantable middle ear hearing devices. Audiol. Neurootol. 12, 265–76. doi:10.1159/000101474

Sun, Q., Gan, R.Z., Chang, K.-H., Dormer, K.J., 2002. Computer-integrated finite element modeling of human middle ear. Biomech. Model. Mechanobiol. 1, 109–22. doi:10.1007/s10237-002-0014-z

Tuck-Lee, J.P., Pinsky, P.M., Steele, C.R., Puria, S., 2008. Finite element modeling of acousto-mechanical coupling in the cat middle ear. J. Acoust. Soc. Am. 124, 348–62. doi:10.1121/1.2912438

Volandri, G., Di Puccio, F., Forte, P., Carmignani, C., 2011. Biomechanics of the tympanic membrane. J. Biomech. 44, 1219–36. doi:10.1016/j.jbiomech.2010.12.023

Zhang, X., Gan, R.Z., 2011a. A comprehensive model of human ear for analysis of implantable hearing devices. IEEE Trans. Biomed. Eng. 58, 3024–3027. doi:10.1109/TBME.2011.2159714

Zhang, X., Gan, R.Z., 2011b. Experimental measurement and modeling analysis on mechanical properties of incudostapedial joint. Biomech. Model. Mechanobiol. 10, 713–26. doi:10.1007/s10237-010-0268-9

Zhao, F., Koike, T., Wang, J., Sienz, H., Meredith, R., 2009. Finite element analysis of the middle ear transfer functions and related pathologies. Med. Eng. Phys. 31, 907–16. doi:10.1016/j.medengphy.2009.06.009

Zilske, M., Lamecker, H., Zachow, S., 2008. Adaptive Remeshing of Non-Manifold Surfaces. Eurographics 2008 Annex to Conf. Proc. 27, 211–214.